

# PCCP

Accepted Manuscript



This is an *Accepted Manuscript*, which has been through the Royal Society of Chemistry peer review process and has been accepted for publication.

*Accepted Manuscripts* are published online shortly after acceptance, before technical editing, formatting and proof reading. Using this free service, authors can make their results available to the community, in citable form, before we publish the edited article. We will replace this *Accepted Manuscript* with the edited and formatted *Advance Article* as soon as it is available.

You can find more information about *Accepted Manuscripts* in the [Information for Authors](#).

Please note that technical editing may introduce minor changes to the text and/or graphics, which may alter content. The journal's standard [Terms & Conditions](#) and the [Ethical guidelines](#) still apply. In no event shall the Royal Society of Chemistry be held responsible for any errors or omissions in this *Accepted Manuscript* or any consequences arising from the use of any information it contains.

# Stabilities and Electronic Properties of Monolayer MoS<sub>2</sub> with One or Two Sulfur Line Vacancy Defects

Yang Han<sup>1</sup>, Ting Hu<sup>1</sup>, Rui Li<sup>1</sup>, Jian Zhou<sup>2</sup> and Jinming Dong<sup>1,a)</sup>

<sup>1</sup>Group of Computational Condensed Matter Physics, National Laboratory of Solid State Microstructures and Department of Physics, Nanjing University, Nanjing 210093, P. R. China

<sup>2</sup>National Laboratory of Solid State Microstructures and Department of Materials Science and Engineering, Nanjing University, Nanjing 210093, P. R. China

## ABSTRACT

Stimulated by the recent experimental observation that single sulfur vacancies in monolayer MoS<sub>2</sub> are mobile under the electron beam and easily agglomerate into the sulfur line vacancy defects [Physical Review B **88**, 035301(2013)], the stabilities and electronic properties of monolayer MoS<sub>2</sub> with one or two staggered sulfur line vacancy defects (SV or DV), along the armchair or zigzag direction (AC-SV, AC-DV or ZZ-SV, ZZ-DV), have been investigated systematically by first-principles calculations. It is found that: **1)** The ZZ-types (ZZ-SV and ZZ-DV) are more stable at different line vacancy densities than the AC-types (AC-SV and AC-DV), in good agreement with previous experimental findings. **2)** More interestingly, it is predicted from our numerical calculations that in the same ZZ-types, the ZZ-DV is more stable than the ZZ-SV, indicating that two separate ZZ-SV line vacancy defects tend to move closely to each other for coalescing into a ZZ-DV, in contrast to the AC-type with AC-SV being a little more stable than the AC-DV. **3)** The monolayer MoS<sub>2</sub> with the AC-SV or AC-DV are both semiconductors with a direct or an indirect band gap, respectively, both of which are much smaller than that of the perfect monolayer. **4)** Furthermore, the out-of-plane distortion induced by the strain release in the monolayer MoS<sub>2</sub> with ZZ-SV or ZZ-DV is more severe than that with the AC-type, which can further decrease the system's gap

<sup>a)</sup>Corresponding author: [jdong@nju.edu.cn](mailto:jdong@nju.edu.cn)

value seriously or even make the gap nearly closed. Our calculation results will be helpful in future nanoelectronics and nanoelectromechanics based on MoS<sub>2</sub> materials.

**KEY WORDS:** stability, electronic property, monolayer MoS<sub>2</sub>, sulfur line vacancy defect

## I. INTRODUCTION

A new novel two dimensional (2D) graphene-like material—monolayer MoS<sub>2</sub><sup>1</sup> has recently become a hot topic in scientific community due to its promising applications in nanoelectronics and optoelectronics<sup>2</sup>. Its intrinsic direct band-gap<sup>1</sup> and good photoluminescence<sup>3-5</sup> have made it a good complimentary material to the semimetal graphene with an intrinsic zero band-gap<sup>6</sup>, which thus hinders its practical applications in the next generation of nanoelectronics and optoelectronics devices.

Monolayer MoS<sub>2</sub> has a layered structure different from that of graphene<sup>7</sup> and h-BN<sup>8</sup>, because it has three atomic layers composed of one Mo layer plus two S layers in both sides. Correspondingly, its bulk structure can be formed by stacking its monolayer through weak van der Waals interaction. In recent years, very thin MoS<sub>2</sub> films and even monolayer structure, prepared on a substrate<sup>9-12</sup> or freely suspended<sup>1, 13</sup> have been successfully realized in experiments by several methods, such as through the micromechanical cleavage technique<sup>1, 13</sup>, chemical exfoliation of the bulk sample<sup>3, 14</sup>, as well as by chemical vapor deposition (CVD)<sup>9, 15-17</sup>.

On the other hand, the topological defects, such as the line defects, dislocations and grain boundaries, exist inevitably in the graphene, h-BN and monolayer MoS<sub>2</sub>, which have an important effect on their physical properties, and correspondingly already been investigated theoretically and experimentally<sup>18-20</sup>. For instance, the grains and grain boundaries composed of the sets of squares and octagons (4–8) or pentagons and heptagons (5–7) defects in the MoS<sub>2</sub> sheet have been recently proposed and observed in experiments by the CVD method<sup>15, 18, 21</sup>. Recently, Duy Le *et al.* have investigated the vacancy structures on one side of monolayer MoS<sub>2</sub> by the density function theory calculations, finding that the formation energy per sulfur vacancy is the lowest (energetically favorable) if the vacancies form a row and the longer the vacancy row, the

lower the formation energy value<sup>22</sup>.

Additionally, two new kinds of sulfur line defects composed of one or two lines of sulfur vacancies has been recently proposed from both experimental results and corresponding theoretical calculations<sup>23</sup>, in which the production, diffusion, and agglomeration of sulfur vacancies in monolayer MoS<sub>2</sub> under electron irradiation have been studied. Particularly, the single vacancies (SVs) are found to be mobile under the electron beam and tend to agglomerate into SV lines, which must have a big effect on the electronic and magnetic properties of defective monolayer MoS<sub>2</sub>.

Therefore in this paper, we have explored the fascinating stability and electronic properties of a monolayer MoS<sub>2</sub> with one or two staggered sulfur line vacancy defects along the zigzag or armchair direction by the first-principles calculations. It is found that monolayer MoS<sub>2</sub> with sulfur line vacancy defects along the ZZ direction are more stable at different line vacancy densities than the AC-types, in good agreement with previous experimental findings. Besides, the monolayer MoS<sub>2</sub> with the sulfur line vacancy defects can behave as a semiconductor with very different gap values, sensitively depending on the direction and density of the line defects.

Furthermore, the out-of-plane distortion induced by the strain release in the monolayer MoS<sub>2</sub> with sulfur line vacancy defects along the ZZ direction is more severe than that with the AC-types, which can further decrease the system's gap value seriously or even make the gap nearly closed. All these important results could provide a new route of tuning the electronic properties of monolayer MoS<sub>2</sub> and its derivatives for their promising applications in nanoelectronics and optoelectronics.

The rest of this paper is organized as follows. In Sec. **II**, we introduce the model and computational details. In Sec. **III**, the main results are given and discussed. Finally, in Sec. **IV**, the conclusions of our work are drawn.

## II. MODEL AND METHOD

The monolayer MoS<sub>2</sub> is modeled by a 2D periodic boundary condition, in which its armchair and zigzag directions are taken along the x and y axes, respectively. The structures of it, viewed from top, AC and ZZ directions are shown in **Fig. 1(a)**, left panel of **Fig. 1(b)** and the top panel of **Fig. 1(c)**, respectively. In order to investigate the sulfur line vacancy defect in monolayer MoS<sub>2</sub> along its AC or ZZ direction, an enlarged rectangle supercell, including two basic unit cells with total two Mo and four S atoms, is chosen as a basic unit in our calculations. The supercell structure and its corresponding first BZ are shown in **Figs. 1(a)** and **1(d)**, respectively.

In this paper, following the previous experimental and theoretical results, only two types of sulfur line vacancy defects are considered, among which one is single sulfur line vacancy defect (SV) and the other is double sulfur line vacancy defect (DV) in a staggered configuration<sup>23</sup>. Because the line vacancy defect orientation can be taken along the AC or ZZ direction, there can be four types of defective monolayer MoS<sub>2</sub> with the sulfur line vacancy defects, denoted by AC-SV, AC-DV, ZZ-SV and ZZ-DV, respectively.

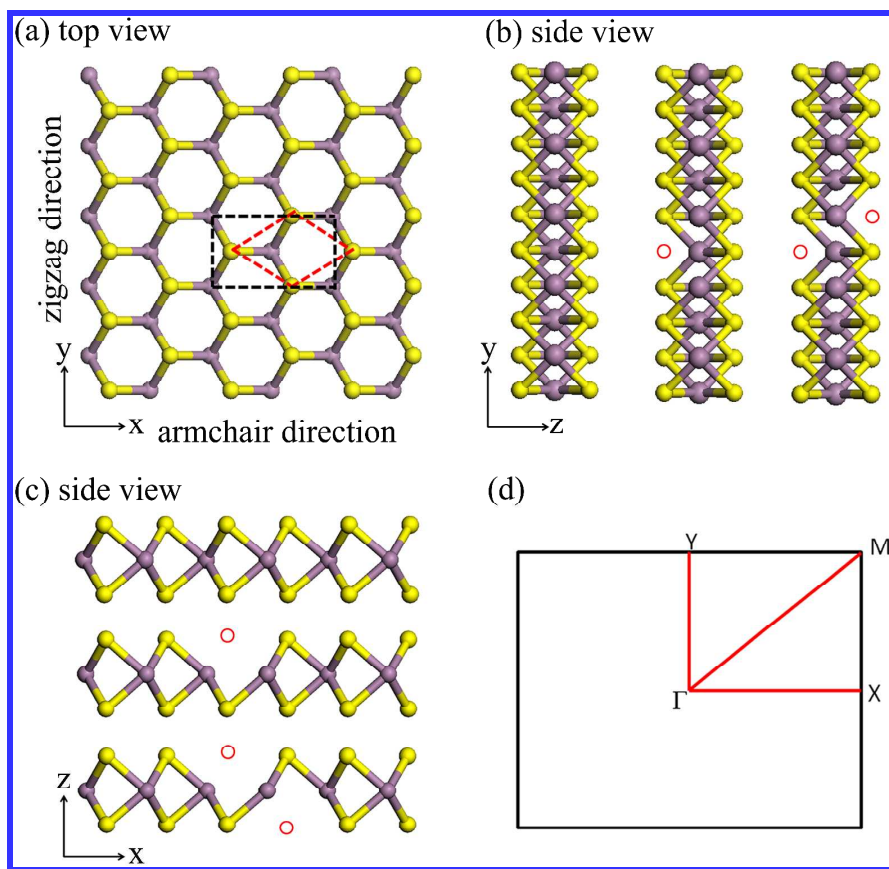


**Fig. 1** (Color online) Geometric structure of a perfect monolayer MoS<sub>2</sub> viewed from out-of-plane z axis, in-plane x and y axes are clearly shown in (a), left panel of (b) and top panel of (c), respectively. The basic unit cell and the rectangle supercell are outlined with red and black dashed lines, respectively. Schematic shows of the defective monolayer MoS<sub>2</sub> with: (b) one (middle panel) and two (right panel) sulfur line vacancy defects along armchair direction, (c) one (central panel) and two (bottom panel) sulfur line vacancy defects along zigzag direction. Red opened circles denote the initial S vacancy positions. Here and hereafter, the Mo and S atoms are represented by purple and yellow balls, respectively. (d) Schematic show of the first Brillouin zone (BZ).

For example, if one sulfur line is deleted from a perfect monolayer MoS<sub>2</sub> along its AC direction, an AC-SV line vacancy defect structure can be formed, as shown in the middle panel of **Fig. 1(b)**, which can be denoted as “AC-SV-MoS<sub>2</sub>-N”, where the integer N represents the number of armchair Mo-S chains between two nearest AC-SV line vacancy defects in the sample. Thus, the sulfur line vacancy defect density in a defective

monolayer MoS<sub>2</sub> can be adjusted by changing the number of N. Similarly, other three types of the sulfur line vacancy defect structures, AC-DV, ZZ-SV and ZZ-DV, are shown, respectively, in the right panel of **Fig. 1(b)**, the middle and lower panels of **Fig. 1(c)**.

We have performed the density functional theory (DFT) calculations in the generalized gradient approximation (GGA) by the Perdew–Burke–Ernzerhof (PBE) exchange-correlation<sup>24</sup>, implemented with the Vienna Ab-initio Simulation Package (VASP)<sup>25-28</sup>, in which the projected augmented wave method<sup>29,30</sup> is adopted. A kinetic energy cutoff of 350 eV for the plane-wave basis set is employed. The 5s<sup>1</sup>4d<sup>5</sup> orbitals of the Mo atom and the 3s<sup>2</sup>3p<sup>4</sup> orbitals of the S atom are treated as valence ones. A large enough vacuum region in Z direction (15 Å) is added in order to make spurious interactions between two nearest samples negligible.

We utilize the Monkhorst–Pack k-point meshes of the 21×1×1 and 1×21×1 unit cells for the first Brillouin zone (BZ) summation when the sulfur line defects are oriented in the AC (x) and ZZ (y) directions, respectively, in order to ensure energy convergence in optimizing structures and total energy calculations. All atoms and the supercell in x and y directions are fully relaxed. Geometric structure optimizations are performed by using the conjugate-gradient algorithm with the maximum residual force at each atom less than 0.02 eV/Å. The allowed error in total energy for the electron self-consistent loop is 10<sup>-5</sup> eV. A much denser k points are used to calculate the band structure.

### III. RESULTS AND DISCUSSIONS

#### A. Geometrical structures of monolayer MoS<sub>2</sub> with sulfur line vacancy defects

Firstly, we have studied the geometric structures of monolayer MoS<sub>2</sub> with sulfur line vacancy defect at different line defect densities. Taking as examples, the optimized

geometric structures of the AC-SV-MoS<sub>2</sub>-8, AC-DV-MoS<sub>2</sub>-8, ZZ-SV-MoS<sub>2</sub>-6, ZZ-SV-MoS<sub>2</sub>-8 and ZZ-DV-MoS<sub>2</sub>-8 are shown in **Figs. 2(a)-(d)** and **2(f)**, respectively. We can see from **Figs. 2(a)** and **2(b)** that the optimized geometric structures of the AC-SV-MoS<sub>2</sub>-8 and AC-DV-MoS<sub>2</sub>-8 almost keep their plane ones, but those of the ZZ-SV-MoS<sub>2</sub>-N and ZZ-DV-MoS<sub>2</sub>-N are found to wrinkle more or less in the out-of-plane direction, as shown in **Figs. 2(c)**, **2(d)** and **2(f)**. In order to study the wrinkle effects on the physical properties, such as the electronic band structure, we have also optimized the ZZ-SV-MoS<sub>2</sub>-8 under a constraint of all Mo atoms lying in the xy plane, and the obtained structure is shown in **Fig. 2(e)**. The fully optimized ZZ-SV-MoS<sub>2</sub>-8 without any constraint shows a big distortion, as can be seen from a comparison of **Figs. 2(d)** and **2(e)**.

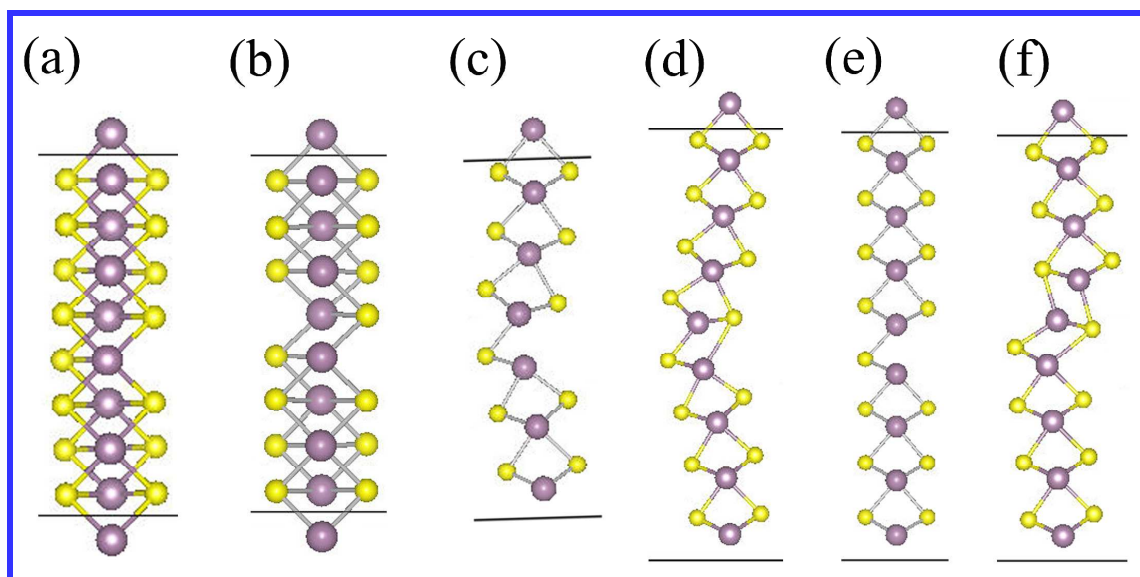


**Fig. 2** (Color online) The side views of the fully optimized geometric structures of the AC-SV-MoS<sub>2</sub>-8, AC-DV-MoS<sub>2</sub>-8, ZZ-SV-MoS<sub>2</sub>-6, ZZ-SV-MoS<sub>2</sub>-8 and ZZ-DV-MoS<sub>2</sub>-8, are given in **(a)-(d)** and **(f)**, respectively. **(e)** That of the ZZ-SV-MoS<sub>2</sub>-8 under a constraint of all Mo atoms lying in xy plane.

## B. Strains in constrained monolayer MoS<sub>2</sub> with sulfur line vacancy defects

It is noted from **Figs. 2(a)** and **2(d)** that the out-of-plane distortion of the ZZ-SV-MoS<sub>2</sub>-8 is more severe than that of the AC-SV-MoS<sub>2</sub>-8. To explain this interesting phenomenon, we have calculated the strain distributions of the Mo-S bonds in the optimized ZZ-SV-MoS<sub>2</sub>-N and AC-SV-MoS<sub>2</sub>-N with all Mo atoms constrained in the xy plane.

The strain of a bond is defined as  $s = \frac{l-l_0}{l_0}$ , where  $l$  is the Mo-S bond length in the constrained defective MoS<sub>2</sub> plane, and  $l_0$  is that in a perfect monolayer MoS<sub>2</sub>. Therefore, the  $s$  value, being larger, smaller than or equal to zero, will be able to indicate that the bond is strained, compressed or not changed, compared with that of a perfect monolayer MoS<sub>2</sub>, which will be denoted by red, blue and white, respectively.

Here, taking as examples, the bond strain distributions in the constrained AC-SV-MoS<sub>2</sub>-8 and ZZ-SV-MoS<sub>2</sub>-8 are shown in **Fig. 3**, from which it can be seen that the severely compressed or strained bonds mainly locate at or near the sulfur line vacancy defect, shown by blue and red colors, respectively. For the constrained AC-SV-MoS<sub>2</sub>-8 in **Fig. 3(a)**, the most severely strained bond is lengthened by 1.2%, denoted by number 1, in contrast to the most severely compressed bond which is shortened by 2%, denoted by number 2.

In comparison, the maximum bond strain and compression for the constrained ZZ-SV-MoS<sub>2</sub>-8, indicated by the numbers 1' and 2' in **Fig. 3(b)**, are 4.6% and 2.6%, respectively, both of which are larger than those values of the constrained AC-SV-MoS<sub>2</sub>-8. Therefore, the released bond strain and compression when the defective MoS<sub>2</sub> plane is optimized in free standing case will cause the out-of-plane distortion of the defective monolayer MoS<sub>2</sub>, which will be more severe for the ZZ-SV-MoS<sub>2</sub>-8 than the AC-SV-MoS<sub>2</sub>-8. Besides, the bond strain and compression for the AC-SV-MoS<sub>2</sub>-8 satisfy the mirror symmetry relative to the sulfur line vacancy due to its intrinsic symmetric

defective structure.

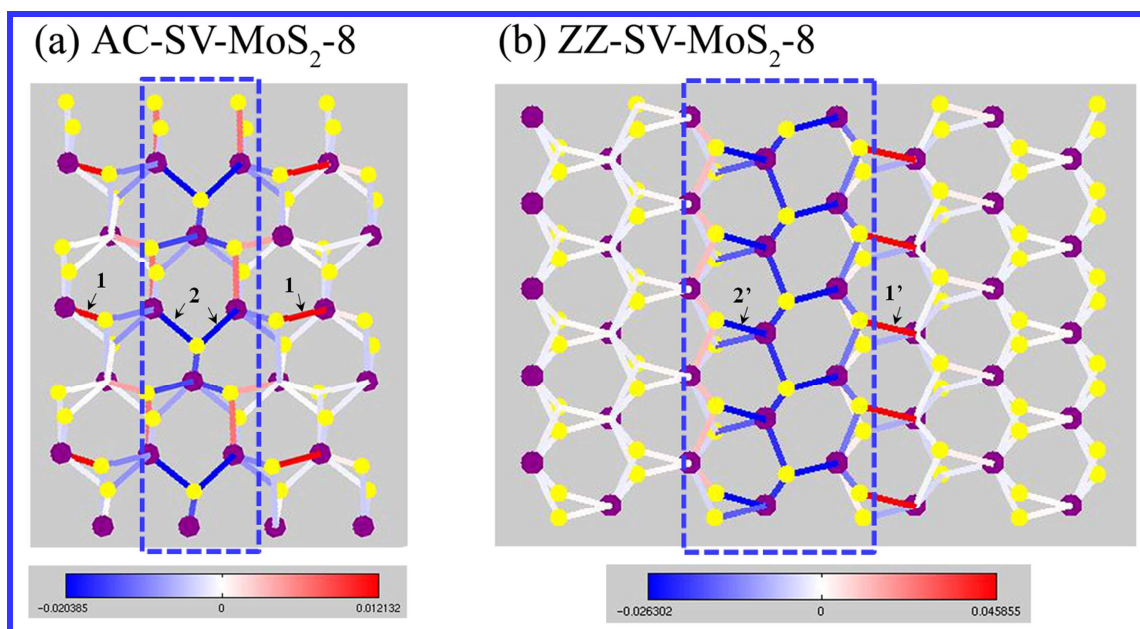


**Fig. 3** (Color online) The bond strain distributions of the optimized (a) AC-SV-MoS<sub>2</sub>-8 and (b) ZZ-SV-MoS<sub>2</sub>-8 under a constraint of all Mo atoms in xy plane. The red or blue colors represent the tensile or compressive Mo-S bonds, compared with the value of 2.41 Å in a perfect monolayer MoS<sub>2</sub>. The color bar is shown at bottom with the maximum tension and compression values of bonds at two ends. The corresponding maximum bonds in defective area are marked by black arrows. The blue rectangle box indicates the defective area.

### C. Stability of sulfur line vacancy defect embedded in monolayer MoS<sub>2</sub>

It is known from the recent experimental result that only two kinds of sulfur line vacancy defects were observed, both of which are along the zigzag direction<sup>23</sup>. So it is very interesting to ask why the sulfur line vacancy defects prefer to take along the zigzag direction?

To answer this question, the stability of 2D monolayer MoS<sub>2</sub> embedded by the sulfur

line vacancy defects along different orientations have been investigated by calculating the formation energy per sulfur vacancy  $E_f$ , which is defined as:

$$E_f = \frac{E_t + N_{\text{Defect-S}} E_S - E_{\text{Ref}}}{N_{\text{Defect-S}}}$$

Here,  $E_t$  and  $E_{\text{Ref}}$  is the total energy per super cell of the sample with and without the sulfur line vacancy defect,  $N_{\text{Defect-S}}$  is the number of S vacancy in the supercell with the sulfur line vacancy defect, and  $E_S$  is the total energy of an isolated sulfur atom. The formation energies of monolayer MoS<sub>2</sub> embedded by the AC- or ZZ-types of sulfur line vacancy defects have been calculated at different line vacancy defect densities, and the obtained results are given in **Fig. 4**.

Firstly, it is found that  $E_f$  of the sulfur line vacancy defects along the ZZ directions (ZZ-SV and ZZ-DV) are both much smaller than those of corresponding AC types (AC-SV and AC-DV) at all different line vacancy defect densities, indicating that the sulfur line vacancy defects along the ZZ direction are more stable than those along the AC direction. This result is in excellent agreement with the previous experimental observations, in which only the sulfur line vacancy defects along the ZZ directions formed under the electron beam<sup>23</sup>. Additionally, our calculation result also coincides with previous work of D. Le *et al.*<sup>22</sup>, in which it was shown that the sulfur vacancies like to sit next to each other, thus forming the ZZ-type sulfur line vacancy defects but not the AC-type ones, because the sulfur vacancies in AC-type vacancy row are separated by other sulfur atoms.

Besides, it is more interesting to find from **Fig. 4** that in the same ZZ-type, the ZZ-DV is more stable than the ZZ-SV. That means two separate ZZ-SVs tend to move closely to each other for coalescing into a ZZ-DV, which is believed to be observed in future experiments. In order to further demonstrate this point, we have optimized the totally eight ZZ-D<sub>n</sub>-MoS<sub>2</sub>-16 in fully free standing cases or under the constraint of all Mo

atoms lying in Mo-planes. Here, the number  $n$  denotes the separated unit distance between two single S line defects along  $x$  axis in **Fig. 1(c)**, where the unit distance is defined as that between two nearest S atoms along  $x$  axis. The calculated total energies of them in free standing cases are found to be always smaller than those corresponding ones under the constraint. Also, the total energy of the  $ZZ-DV_n$ -MoS<sub>2</sub>-16 at  $n=1$ , forming one  $ZZ-DV$ , is smaller than those at  $n \geq 3$  with still two separate single sulfur line vacancy defects. For example, in free standing cases, the  $ZZ-DV_1$ -MoS<sub>2</sub>-16 (one  $ZZ-DV$ ) is 57.13 meV lower in energy than  $ZZ-DV_8$ -MoS<sub>2</sub>-16 (with two separated  $ZZ-SVs$ ). But under the constraint condition, the energy difference between both of them becomes even larger, which is found to be 311 meV. Our calculation results prove clearly that two  $ZZ-SVs$  indeed like to merge into a  $ZZ-DV$ , when they move close to each other. However, as seen from **Fig. 4**, in the same AC-type, the AC-SV is found to be a little bit more stable than the AC-DV at all different line vacancy defect densities, which is just opposite to the  $ZZ$ -type situation given above. This fact tell us that the  $ZZ-DV$  line vacancy defect is more easily formed in experiment, in contrast to the AC-SV being more easily formed.

Finally,  $E_f$  of the DV-type (AC-DV and  $ZZ-DV$ ) and the AC-SV do not almost vary with the line vacancy defect densities, in distinct contrast to that of the  $ZZ-SV$ , which decreases slowly with the number  $N$  (or with the decreasing of SV line vacancy defect density). A possible reason is that the heavier out-of-plane distortion induced by more strain release in the  $ZZ-SV$  type with the larger number  $N \geq 8$  will lead to a lower formation energy and more stable structure.

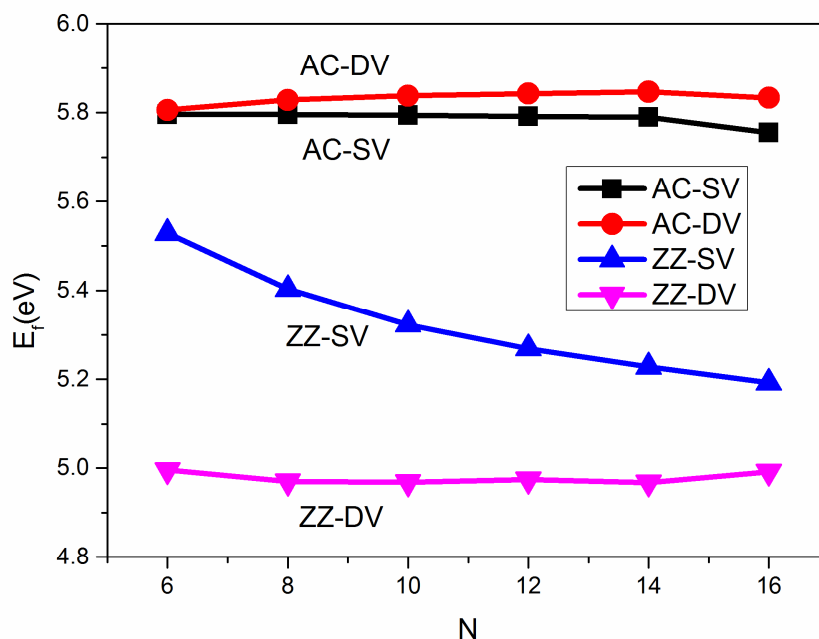


**Fig. 4** (Color online) Formation energies of the SV and DV types of sulfur line vacancy defects in monolayer MoS<sub>2</sub> along the AC or ZZ direction versus different numbers of N.

#### D. Electronic properties of monolayer MoS<sub>2</sub> with sulfur line vacancy defect along the AC direction

Based upon the optimized geometric structures of the defective monolayer MoS<sub>2</sub> with the different types of sulfur line vacancy defects, we have calculated their electronic structures systematically. The obtained results are given in **Fig. 5**, showing very interesting semiconductor or mini-gap properties of them. It is seen from **Fig. 5(a)** and **5(b)** that the AC-SV-MoS<sub>2</sub>-8 and AC-DV-MoS<sub>2</sub>-8 both behave as semiconductors with a direct band gap of ~ 0.87 eV and an indirect one of ~ 0.23 eV, respectively, which are much smaller than that (1.68 eV) of a perfect monolayer MoS<sub>2</sub> because the line vacancy defect introduces ‘impurity’ states into its original band gap, denoted by blue solid squares in the band structures of **Fig. 5(a)** and **5(b)**.

For example, for the AC-SV-MoS<sub>2</sub>-8, the *a*, *b* and *c* states, shown in **Fig. 5(a)**, are very localized and mainly contributed by the d orbitals of the Mo atoms at the line defects. Both the valence band maximum (VBM) and the conduction band minimum (CBM) locate at the  $\Gamma$  point of the first BZ, creating so a direct band gap. In **Fig. 5(g)**, the corresponding integrated charge density of the defect states, *a*, *b* and *c* are also plotted. From **Fig. 5(g)**, it is found that the three defect states are mainly focused on the Mo atoms nearby the sulfur vacancies. The defect valence state *a* locates at the same line of Mo atoms with the sulfur vacancies (left part of the top panels in **Fig. 5(g)**), in contrast to the defect conduction band *b* sitting on both the neighboring lines of Mo atoms to the sulfur line vacancy defect (the middle part of the top panels in **Fig. 5(g)**). On the other hand, the 3<sup>rd</sup> localized conduction state—band *c* in **Fig. 5(a)** is contributed by nearly all lines of Mo atoms in the defect areas, which can be seen clearly from the right part of the top panels in **Fig. 5(g)**.

In contrast, the CBM of the AC-DV-MoS<sub>2</sub>-8 in **Fig. 5(b)** moves close to Y point, leading to its indirect gap. As seen from **Fig. 5(b)**, there are more defect states for the AC-DV-MoS<sub>2</sub>-8 than its SV counterpart, thereby leading to a much smaller band gap for the AC-DV-MoS<sub>2</sub>-8. By analyzing the band structure, it is found that all defect states are also mainly contributed by the d orbitals of the Mo atoms at the sulfur line vacancy defects.

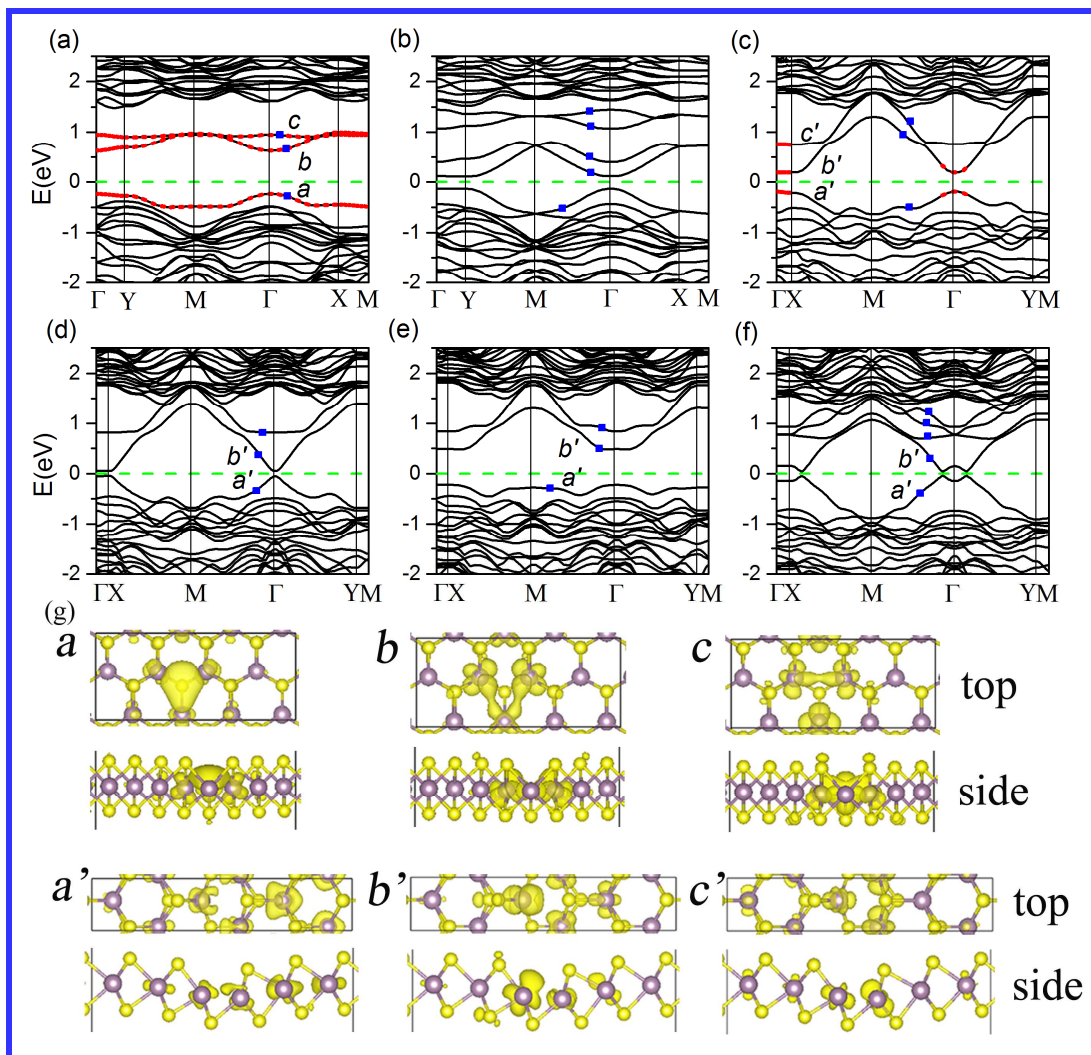


**Fig. 5** (Color online) The band structures of: **(a)** AC-SV-MoS<sub>2</sub>-8, **(b)** AC-DV-MoS<sub>2</sub>-8, **(c)** ZZ-SV-MoS<sub>2</sub>-6, **(d)** ZZ-SV-MoS<sub>2</sub>-8, **(e)** ZZ-SV-MoS<sub>2</sub>-8 with Mo atoms constrained in the xy plane and **(f)** ZZ-DV-MoS<sub>2</sub>-8, respectively. The Fermi level is set to zero. The defect states are denoted by blue solid squares in **(a)-(f)**. The k points indicated by the red solid circles on the defect states, shown in **(a)** and **(c)**, are selected to calculate the integrated charge densities of the defect states. **(g)** gives the integrated charge densities of the defect states of *a*, *b* and *c* in **(a)** and *a'*, *b'* and *c'* in **(c)**, in which the isovalues for these isosurfaces are taken as  $0.03 \text{ e}/\text{\AA}^3$  for the *a*, *b*, *c* and  $0.01 \text{ e}/\text{\AA}^3$  for the *a'*, *b'*, *c'*.

## E. Electronic properties of monolayer MoS<sub>2</sub> with sulfur line vacancy defect along the ZZ direction

Now, let's turn to the ZZ type cases, which are found to be semiconductors with very different band gap values, depending on the line vacancy defect densities and line vacancy types, as seen from **Fig. 5(c)**, **5(d)** and **5(f)**. The fact that ZZ-SV or ZZ-DV may have very small band-gap was also reported by Komsa *et al.*<sup>23</sup>. It is more interesting to find that the band gap of ZZ-SV-MoS<sub>2</sub>-N decreases drastically with increasing the number of N.

For example, the ZZ-SV-MoS<sub>2</sub>-6 is a good semiconductor with an indirect band gap of 0.384 eV. Its VBM lies at the  $\Gamma$  point and its CBM does at the X point, as seen from **Fig. 5(c)**. The integrated charge densities of flat parts for the defect bands *a'*, *b'* and *c'* of **Fig. 5(c)** are shown in the bottom panels of **Fig. 5(g)**, indicating that the charge densities on the flat parts are mainly localized on the Mo atoms near the sulfur line vacancy defect.

However, it is noted that the ZZ-SV-MoS<sub>2</sub>-8 has a very small indirect band gap of about 99 meV, as shown in **Fig. 5(d)**. This nearly-closed band gap of the ZZ-SV-MoS<sub>2</sub>-8 is caused by the close movement of its two neighbor defect states *a'* and *b'* on both sides of the Fermi level, compared with those of the ZZ-SV-MoS<sub>2</sub>-6. We have also tested the bigger number of N for the ZZ-SV-MoS<sub>2</sub>-N, and found the similar behavior with a nearly-closed band gap. It is noted from our numerical calculations that the ZZ-SV-MoS<sub>2</sub>-N with the bigger number  $N \geq 8$  will wrinkle much more heavily, compared with those having the smaller number  $N \leq 6$ . The larger the wrinkles, the heavier their effects on the electronic structures of ZZ-SV-MoS<sub>2</sub>-N.

In order to study the wrinkle effect on the band gap of ZZ-SV-MoS<sub>2</sub>-N in more detail, we have optimized the ZZ-SV-MoS<sub>2</sub>-8 under a constraint of all Mo atoms in xy plane, and the obtained geometric structure is shown in **Fig. 2(e)**. And the calculated electronic band structure of it is shown in **Fig. 5(e)**, from which we can see clearly that the constrained ZZ-SV-MoS<sub>2</sub>-8 is also a semiconductor, but has a much larger indirect band gap of 0.702 eV.

In contrast, the unconstrained ZZ-SV-MoS<sub>2</sub>-8 has a much smaller indirect band gap of 0.099 eV. That is because the defect states— $a'$  and  $b'$  of the constrained ZZ-SV-MoS<sub>2</sub>-8 move far away from the Fermi level, compared with the band structure of the fully optimized one, shown in **Fig. 5(d)**. The above results clearly demonstrate that the deep decrease of the band gap value of the ZZ-SV-MoS<sub>2</sub>-N with the bigger number  $N \geq 8$  is mainly caused by its larger out-of-plane structure deformation (or wrinkles) in the fully free standing case.

Finally, the monolayer MoS<sub>2</sub> with two sulfur line vacancy defects (DV) along its zigzag direction has been investigated. Taking the ZZ-DV-MoS<sub>2</sub>-8 as an example, its band structure is shown in **Fig. 5(f)**, indicating that it has an indirect band gap with a nearly negligible value of 94 meV. This very small band gap is caused mainly by two reasons. One is that the DV type of sulfur line vacancy defect induces more defect states near the Fermi level, compared with the band structure of the corresponding SV one. The other is that the out-of-plane structural distortion, as explained above, makes two defect states of  $a'$  and  $b'$  closely move to the Fermi level, thus leading to a smaller band gap value.

#### IV. SUMMARY

The stabilities, geometric and electronic structures of the monolayer MoS<sub>2</sub> with one or two staggered sulfur line vacancy defects, parallel to the AC or ZZ direction, have been investigated systematically by the first principles calculations. It is interesting to find that the sulfur line vacancy defects along the ZZ direction (both the ZZ-SV and ZZ-DV) are more stable at different line vacancy defect densities than those along the AC direction, which is well consistent with the previous experimental observations. More interestingly, in the same ZZ-type, the ZZ-DV is found to be more stable than the ZZ-SV, indicating that two separate ZZ-SV line vacancy defects tend to move closely to each other for coalescing into a ZZ-DV one. In contrast, in the same AC-type, the AC-SV is a

little more stable than the AC-DV.

Besides, both the AC-SV-MoS<sub>2</sub> and AC-DV-MoS<sub>2</sub> behave as semiconductors with their gap values much smaller than the perfect monolayer MoS<sub>2</sub> due to the introduction of impurity states in their original band gaps. Moreover, the out-of-plane distortions in the defective monolayer MoS<sub>2</sub> with the ZZ-SV or ZZ-DV sulfur line vacancy defects are more severe than those with the AC-type due to much more strain releases in the former ones, which would decrease their gap values seriously or even lead to nearly closed band gaps. In a word, our obtained results will be helpful for applications of the defective monolayer MoS<sub>2</sub> materials in future nanoelectronics and electromechanical devices.

## ACKNOWLEDGEMENT

The authors acknowledge financial supports from the State Key Program for Basic Research of China through the Grant Nos. 2010CB630704, and 2011CB922100Q. Our numerical calculations are performed on the High Performance Computing Center of Nanjing University. Y. Han gratefully acknowledge useful discussions with Dr. Y. P. Du.

## REFERENCES

- 1 K. F. Mak, C. Lee, J. Hone, J. Shan, T. F. Heinz, *Physical Review Letters*, 2010, **105**, 136805.
- 2 Q. H. Wang, K. Kalantar-Zadeh, A. Kis, J. N. Coleman, M. S. Strano, *Nature Nanotechnology*, 2012, **7**, 699-712.
- 3 G. Eda, H. Yamaguchi, D. Voiry, T. Fujita, M. W. Chen, M. Chhowalla, *Nano Letters*, 2011, **11**, 5111-5116.
- 4 Q. Q. Ji, Y. F. Zhang, T. Gao, Y. Zhang, D. L. Ma, M. X. Liu, Y. B. Chen, X. F. Qiao, P. H. Tan, M. Kan, J. Feng, Q. Sun, Z. F. Liu, *Nano Letters*, 2013, **13**, 3870-3877.
- 5 A. Splendiani, L. Sun, Y. B. Zhang, T. S. Li, J. Kim, C. Y. Chim, G. Galli, F. Wang, *Nano Letters*, 2010, **10**, 1271-1275.

- 6 A. H. Castro Neto, F. Guinea, N. M. R. Peres, K. S. Novoselov, A. K. Geim, *Reviews of Modern Physics*, 2009, **81**, 109-162.
- 7 K. S. Novoselov, A. K. Geim, S. V. Morozov, D. Jiang, Y. Zhang, S. V. Dubonos, I. V. Grigorieva, A. A. Firsov, *Science*, 2004, **306**, 666-669.
- 8 D. Pacile, J. C. Meyer, C. O. Girit, A. Zettl, *Applied Physics Letters*, 2008, **92**, 133107.
- 9 Y. Zhan, Z. Liu, S. Najmaei, P. M. Ajayan, J. Lou, *Small*, 2012, **8**, 966-971.
- 10 Y. M. Shi, W. Zhou, A. Y. Lu, W. J. Fang, Y. H. Lee, A. L. Hsu, S. M. Kim, K. K. Kim, H. Y. Yang, L. J. Li, J. C. Idrobo, J. Kong, *Nano Letters*, 2012, **12**, 2784-2791.
- 11 D. Kim, D. Z. Sun, W. H. Lu, Z. H. Cheng, Y. M. Zhu, D. Le, T. S. Rahman, L. Bartels, *Langmuir*, 2011, **27**, 11650-11653.
- 12 G. A. Salvatore, N. Munzenrieder, C. Barraud, L. Petti, C. Zysset, L. Buthe, K. Ensslin, G. Troster, *Acs Nano*, 2013, **7**, 8809-8815.
- 13 J. Wu, H. Li, Z. Yin, H. Li, J. Liu, X. Cao, Q. Zhang, H. Zhang, *Small*, 2013, **9**, 3314-3319.
- 14 J. N. Coleman, M. Lotya, A. O'Neill, S. D. Bergin, P. J. King, U. Khan, K. Young, A. Gaucher, S. De, R. J. Smith, I. V. Shvets, S. K. Arora, G. Stanton, H.-Y. Kim, K. Lee, G. T. Kim, G. S. Duesberg, T. Hallam, J. J. Boland, J. J. Wang, J. F. Donegan, J. C. Grunlan, G. Moriarty, A. Shmeliov, R. J. Nicholls, J. M. Perkins, E. M. Grieverson, K. Theuwissen, D. W. McComb, P. D. Nellist, V. Nicolosi, *Science*, 2011, **331**, 568-571.
- 15 S. Najmaei, Z. Liu, W. Zhou, X. L. Zou, G. Shi, S. D. Lei, B. I. Yakobson, J. C. Idrobo, P. M. Ajayan, J. Lou, *Nature Materials*, 2013, **12**, 754-759.
- 16 Y. H. Lee, L. L. Yu, H. Wang, W. J. Fang, X. Ling, Y. M. Shi, C. T. Lin, J. K. Huang, M. T. Chang, C. S. Chang, M. Dresselhaus, T. Palacios, L. J. Li, J. Kong, *Nano Letters*, 2013, **13**, 1852-1857.
- 17 S. F. Wu, C. M. Huang, G. Aivazian, J. S. Ross, D. H. Cobden, X. D. Xu, *Acs Nano*, 2013, **7**, 2768-2772.
- 18 W. Zhou, X. L. Zou, S. Najmaei, Z. Liu, Y. M. Shi, J. Kong, J. Lou, P. M. Ajayan, B. I. Yakobson, J. C. Idrobo, *Nano Letters*, 2013, **13**, 2615-2622.
- 19 X. L. Zou, Y. Y. Liu, B. I. Yakobson, *Nano Letters*, 2013, **13**, 253-258.

- 20 Z. Zhang, X. Zou, V. H. Crespi, B. I. Yakobson, *ACS nano*, 2013, **7**, 10475-10481.
- 21 A. M. van der Zande, P. Y. Huang, D. A. Chenet, T. C. Berkelbach, Y. M. You, G. H. Lee, T. F. Heinz, D. R. Reichman, D. A. Muller, J. C. Hone, *Nature Materials*, 2013, **12**, 554-561.
- 22 D. Le, T. B. Rawal, T. S. Rahman, *The Journal of Physical Chemistry C*, 2014, **118**, 5346-5351.
- 23 H. P. Komsa, S. Kurasch, O. Lehtinen, U. Kaiser, A. V. Krasheninnikov, *Physical Review B*, 2013, **88**, 035301.
- 24 J. P. Perdew, K. Burke, M. Ernzerhof, *Physical Review Letters*, 1996, **77**, 3865-3868.
- 25 G. Kresse, J. Hafner, *Physical Review B*, 1993, **47**, 558-561.
- 26 G. Kresse, J. Hafner, *Physical Review B*, 1994, **49**, 14251-14269.
- 27 G. Kresse, J. Furthmüller, *Physical Review B*, 1996, **54**, 11169-11186.
- 28 G. Kresse, J. Furthmüller, *Computational Materials Science*, 1996, **6**, 15-50.
- 29 P. E. Blöchl, *Physical Review B*, 1994, **50**, 17953-17979.
- 30 G. Kresse, D. Joubert, *Physical Review B*, 1999, **59**, 1758-1775.

## FIGURE CAPTIONS

**Fig. 1** (Color online) Geometric structure of a perfect monolayer MoS<sub>2</sub> viewed from out-of-plane z axis, in-plane x and y axes are clearly shown in **(a)**, left panel of **(b)** and top panel of **(c)**, respectively. The basic unit cell and the rectangle supercell are outlined with red and black dashed lines, respectively. Schematic shows of the defective monolayer MoS<sub>2</sub> with: **(b)** one (middle panel) and two (right panel) sulfur line vacancy defects along armchair direction, **(c)** one (central panel) and two (bottom panel) sulfur line vacancy defects along zigzag direction. Red opened circles denote the initial S vacancy positions. Here and hereafter, the Mo and S atoms are represented by purple and yellow balls, respectively. **(d)** Schematic show of the first Brillouin zone (BZ).

**Fig. 2** (Color online) The side views of the fully optimized geometric structures of the AC-SV-MoS<sub>2</sub>-8, AC-DV-MoS<sub>2</sub>-8, ZZ-SV-MoS<sub>2</sub>-6, ZZ-SV-MoS<sub>2</sub>-8 and ZZ-DV-MoS<sub>2</sub>-8, are given in **(a)-(d)** and **(f)**,

respectively. (e) That of the ZZ-SV-MoS<sub>2</sub>-8 under a constraint of all Mo atoms lying in xy plane.

**Fig. 3** (Color online) The bond strain distributions of the optimized (a) AC-SV-MoS<sub>2</sub>-8 and (b) ZZ-SV-MoS<sub>2</sub>-8 under a constraint of all Mo atoms in xy plane. The red or blue colors represent the tensile or compressive Mo-S bonds, compared with the value of 2.41 Å in a perfect monolayer MoS<sub>2</sub>. The color bar is shown at bottom with the maximum tension and compression values of bonds at two ends. The corresponding maximum bonds in defective area are marked by black arrows. The blue rectangle box indicates the defective area.

**Fig. 4** (Color online) Formation energies of the SV and DV types of sulfur line vacancy defects in monolayer MoS<sub>2</sub> along the AC or ZZ direction versus different numbers of N.

**Fig. 5** (Color online) The band structures of: (a) AC-SV-MoS<sub>2</sub>-8, (b) AC-DV-MoS<sub>2</sub>-8, (c) ZZ-SV-MoS<sub>2</sub>-6, (d) ZZ-SV-MoS<sub>2</sub>-8, (e) ZZ-SV-MoS<sub>2</sub>-8 with Mo atoms constrained in the xy plane and (f) ZZ-DV-MoS<sub>2</sub>-8, respectively. The Fermi level is set to zero. The defect states are denoted by blue solid squares in (a)-(f). The k points indicated by the red solid circles on the defect states, shown in (a) and (c), are selected to calculate the integrated charge densities of the defect states. (g) gives the integrated charge densities of the defect states of *a*, *b* and *c* in (a) and *a'*, *b'* and *c'* in (c), in which the isovalues for these isosurfaces are taken as 0.03 e/Å<sup>3</sup> for the *a*, *b*, *c* and 0.01 e/Å<sup>3</sup> for the *a'*, *b'*, *c'*.